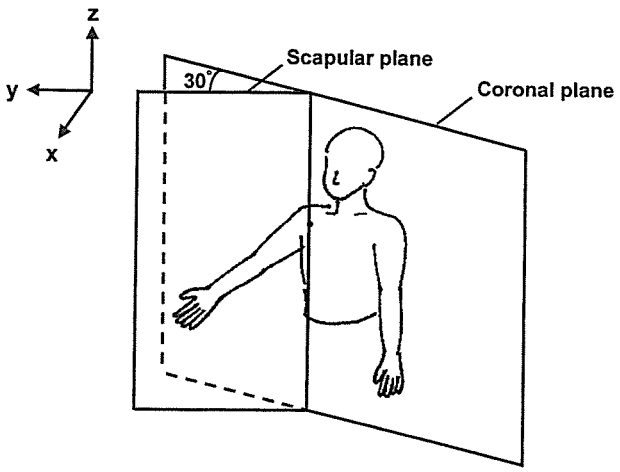


**Figure 1** Three-dimensional coordinate system of model. Origin, Center of humeral head; x-axis, perpendicular to scapular plane; y-axis, horizontal on scapular plane; z-axis, vertical.

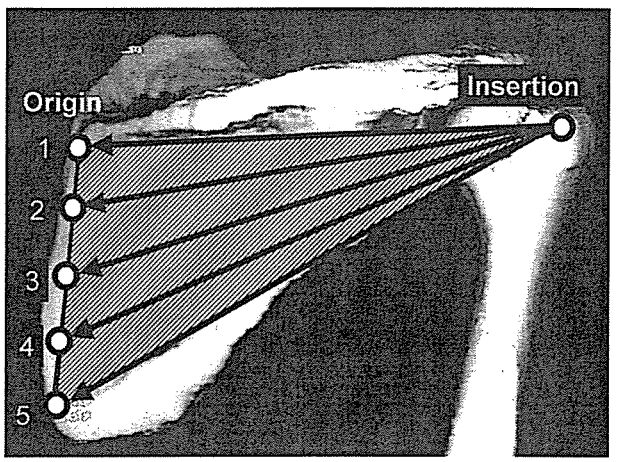


**Figure 2** In the infraspinatus muscle, 5 possible origin points were set on the edge of the origin area at even intervals, and the adequate point was selected in each abduction angle by use of the optimization method.

kee, WI). The slice thickness and interval were set at 1 mm and the table speed at 1 mm/s. The upper extremity was placed at the side of the trunk, the shoulder joint was positioned in neutral rotation, and the elbow joint was positioned in full extension during imaging. The obtained images were transferred to a computer, and a 3-dimensional image was created by use of the medical image–analyzing software Analyze 3.0 (Biomechanical Imaging Resource, Rochester, MN). A 3-dimensional coordinate system was determined, with the center of the humeral head being considered as the origin (Figure 1). Each axis was determined as follows: x-axis, perpendicular to the scapular plane (a vertical plane 0° from a frontal plane); y-axis, horizontal on the scapular plane; and z-axis, vertical. Three-dimensional coordinates of the origin and insertion of each muscle were manually determined from muscle contours or anatomic bony landmarks (or both) on the 3 directional (coronal, sagittal, and axial) cross-sectional images. Every coordinate point was automatically placed on the surface of the bone. Eleven muscles that originate from the scapula and insert on the upper extremity (humerus, radius, and ulna) were included in this study. Those muscles were as follows: anterior fiber of deltoid (F1), middle fiber of deltoid (F2), posterior fiber of deltoid (F3), supraspinatus (F4), infraspinatus (F5), subscapularis (F6), teres minor (F7), teres major (F8), long head of biceps (F9), short head of biceps (F10), and long head of triceps (F11). The muscles were basically defined as a straight-line vector from the insertion to the origin. However, in muscles that originate from a wide area, it is quite unlikely that all muscle fibers transmit the force to the insertion equally during various movements. The most active muscle fibers should change as the joint position changes. Therefore, if these muscles are represented as a fixed straight-line vector, considerable errors may result in the analysis. For these reasons, we assumed that the primary active muscle fibers were approximated to a straight-line vector, which changed its direction in each abduction angle. On the basis of this assumption, we developed the following procedure. An origin line was determined on the edge of the origin area that was farthest from the insertion, and several possible origin points were set on the line at even intervals (Figure 2). Three points were set as possible origin points for each fiber of the deltoid and supraspinatus, and five points were set for the infraspinatus and subscapularis according to the approximate length of the origin line of each muscle. The optimal point in each abduction angle, which determined the direction of the muscle vector, was selected among these points by use of the optimization technique mentioned later. The insertion remained fixed in every muscle. By this procedure, an optimal muscle vector was determined in every abduction angle.

The proximal part of the long head of the biceps shows a unique morphology that originates from the glenoid rim as a tendon and runs along the surface of the humeral head. We set the contact point at the upper end of the bicipital groove and defined the muscle vector as a straight-line vector from the insertion to the contact point, as opposed to defining the vector from the insertion to the origin.

The middle fiber of the deltoid muscle is in a curved shape, wraps around the humeral head in small abduction angles (Figure 3, *A*), and becomes a linear shape as the arm abducts (Figure 3, *B*). Because the straight-line vector from its insertion to the origin penetrates the humerus in small abduction angles, we set the contact point on the greater tuberosity and defined the muscle vector as a vector from the insertion to the contact point as aforementioned. To determine the range of the abduction angle where the straight-line vector penetrates the bone, we carried out the following study: Magnetic resonance imaging data of the shoulders in 10 normal volunteers (8 men and 2 women), including the same volunteer whose CT data were used for the musculoskeletal model, were prepared. The mean age was 24.8 years (range, 24-39 years). All subjects had neither a history of trauma nor any symptoms in the examined shoulders. Informed consent for participating in this study was obtained. Oblique coronal (scapular-plane) views of the shoulders were scanned via an open magnetic resonance scanner (0.2-T Magnetom Open; Siemens, Er-

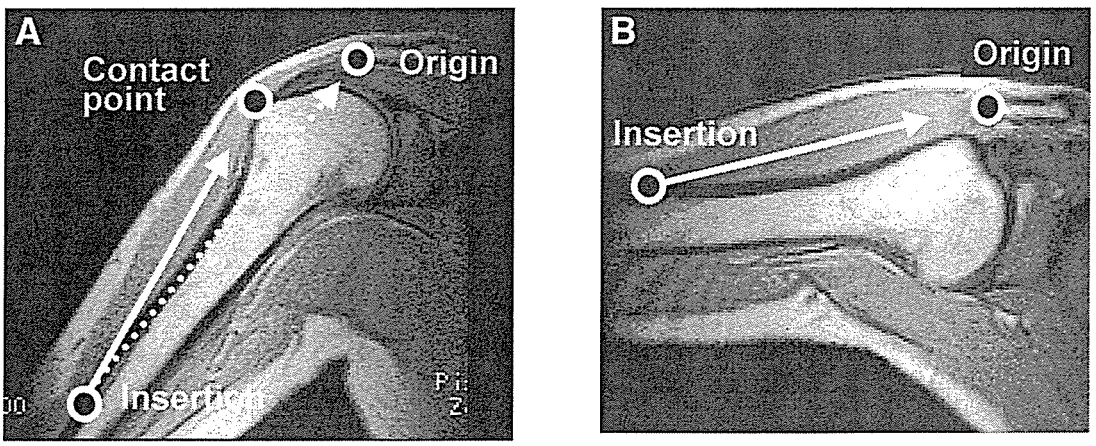


**Figure 3 A**, In the middle fiber of deltoid, the straight-line vector from the insertion point to the origin point penetrates the bone (*dotted arrow*) at 60° abduction and below; therefore, the muscle vector is established from the insertion point to the contact point (*solid arrow*). **B**, The muscle vector is determined from the insertion point to the origin point over 60° abduction (*arrow*).

langen, Germany) with the arm positioned in 30°, 60°, 90°, 120°, and 150° abduction in a scapular plane. A $T_2$-weighted, 2-dimensional gradient-echo sequence was applied (repitition time [TR], 304.0 milliseconds; echo time [TE], 25.9 milliseconds; flip angle, 60°; field of view [FOV], 220 mm$^2$; matrix, 192 × 256; slice thickness, 5 mm). On the image representing the midportion of the middle fiber of the deltoid, a straight line connecting the insertion and the origin was drawn by use of Analyze 3.0 software (Biomechanical Imaging Resource). The slice in which the straight line penetrated the humerus was then studied. As a result, the straight line penetrated the humerus at 60° abduction and below in 8 of 10 subjects, including the volunteer who provided the CT data.

From this result, the muscle vector of the middle fiber of the deltoid was established from the insertion to the contact point at 60° abduction and below and from the insertion to the origin over 60° abduction. Finally, the musculoskeletal model was obtained as shown in Figure 4. A triangular shape demonstrates the muscle with a wide origin area (F1-F6).

The analyzed motion was abduction of the shoulder joint in the scapular plane ranging from 10° to 150°. During abduction, the shoulder joint was kept in neutral rotation, the elbow joint in full extension, and the forearm in neutral rotation. In this model, not only glenohumeral joint motion but also scapulothoracic motion was considered. Motion of the scapula was reproduced according to a previous in vivo study,[9] and all of the coordinate points on the scapula and upper arm were transformed as the position of the scapula changed. The glenohumeral joint was defined as a ball joint, and the center of the humeral head, which was approximated to a sphere, was defined as the center of rotation. The upper extremity was assumed to be a rigid body. The self-weight of the upper extremity, which was defined to be 5.2% of the body weight,[13] was applied at the middle point between the shoulder and wrist joint. The self-weight was considered to be the only external force in this analysis. Internal forces acting on the upper extremity were the muscle forces and the joint reaction force. No

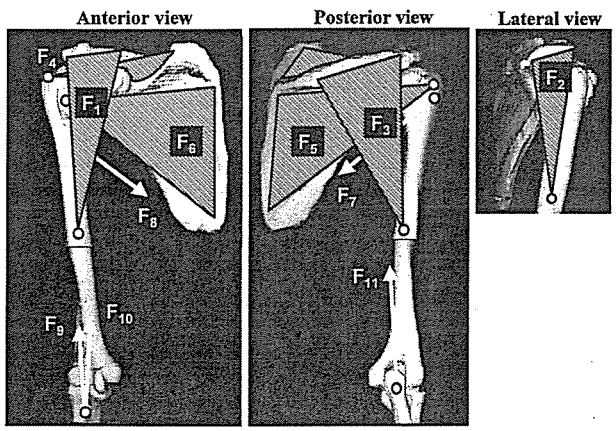


**Figure 4** Musculoskeletal model. The triangular shape represents a wide muscle (F1-F6). *F1*, Anterior fiber of deltoid; *F2*, middle fiber of deltoid; *F3*, posterior fiber of deltoid; *F4*, supraspinatus; *F5*, infraspinatus; *F6*, subscapularis; *F7*, teres minor; *F8*, teres major; *F9*, long head of biceps; *F10*, short head of biceps; *F11*, long head of triceps.

friction at the articular surface was considered. Because the muscle forces and joint reaction force were obtained only from the equilibrium equations of force in this study, any ligaments or capsules that demonstrated no force were not considered.

Three-dimensional static equilibriums on force and moment were formulated by use of force vectors as shown in Figure 5, where $F_i$ indicates the magnitude of the muscle forces, $\vec{W}$ represents the gravity vector of the self-weight of the upper extremity, and $\vec{R}$ represents the reaction force vector. By denoting the unit vector of the muscle forces by $\vec{u}_i$, and the position vector of the action points of the muscle forces, the reaction force, and the self-weight by $\vec{r}_i$, $\vec{r}_r$, and $\vec{r}_w$, respectively, the equilibrium equations on force and moment can be expressed as Equations 1 and 2:

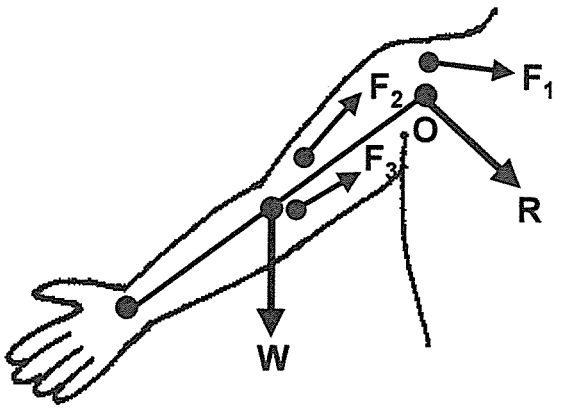


**Figure 5** Three-dimensional biomechanical model for formulation. $F_i$, Each muscle force (i = 1-11); $R$, joint reaction force; $W$, self-weight of upper extremity.

$$\sum_{i=1}^{11} \vec{F_i u_i} + \vec{R} + \vec{W} = 0 \quad (1)$$

$$\sum_{i=1}^{11} (\vec{r_i} \times \vec{F_i u_i}) + \vec{r_r} \times \vec{R} + \vec{r_w} \times \vec{W} = 0 \quad (2)$$

Because a value of muscle force must not be negative, the following expression can be indicated:

$$F_i \geq 0 \quad (3)$$

Six equations derived from Equations 1 and 2 along each of the x-, y-, and z-axes have 14 unknown quantities, which are 11 muscle forces and 3 components of the joint reaction force. This equation system indicates an indeterminate problem with an infinite number of solutions. To find a unique solution, an optimization technique by the successive quadratic programming method was applied. An objective function used in the successive quadratic programming method is defined as the total sum of the square of the muscle stress, which is the muscle force divided by the physiologic cross-sectional area (PCSA), and is expressed as Equation 4:

$$U = \sum_{i=1}^{11} (F_i / PCSA_i)^2 \quad (4)$$

The value of PCSA of each muscle was obtained from a previous study[10] (Table I). The objective function $U$ was minimized by use of Equation 1, Equation 2, and inequality (Equation 3) as the constrained conditions. The optimal origin points of the muscles with a wide origin area were also determined to minimize the objective function at this stage. The static numerical analysis was performed every 5°.

### *EMG*

To validate the results of the computer simulation, we carried out EMG in the same volunteer whose CT data were used to build the musculoskeletal model. The 6-channel Polygraph 360 System (NEC Medical Systems, Tokyo, Japan) was applied for the measurement. Platinum fine-wire electrodes with a diameter of 0.05 mm were used for the supraspinatus, infraspinatus, subscapularis, and teres minor; disposable surface electrodes were used for each fiber of the deltoid, biceps, and triceps. The surface electrodes were attached to the skin over the muscle belly with an inter-electrode center-to-center distance of 30 mm. Abduction movement in the scapular plane from 10° to 150° was statically measured every 10°. The subject was told to stand and hold his upper limb in an abducted position with no extra load for 5 seconds. The position of each joint was matched with the corresponding position of the model. A 1-minute rest period was permitted before changing positions. The data were recorded on a computer by use of Biocorder software (KISSEI COMTEC, Nagano, Japan). For data analysis, the middle 3 seconds of each measurement were selected and integrated by use of BIMUTAS II software (KISSEI COMTEC). The same procedure was repeated 3 times, and the mean value was calculated.

**Table 1** PCSA of the analyzed muscles[10]

| Muscle | PCSA (cm²) |
|---|---|
| F1; Anterior fiber of deltoid | 4.5 |
| F2; Middle fiber of deltoid | 13.5 |
| F3; Posterior fiber of deltoid | 3.9 |
| F4; Supraspinatus | 4.5 |
| F5; Infraspinatus | 5.8 |
| F6; Subscapularis | 9.7 |
| F7; Teres minor | 2.6 |
| F8; Teres major | 5.8 |
| F9; Long head of biceps | 1.9 |
| F10; Short head of biceps | 1.3 |
| F11; Triceps | 3.9 |

PCSA, physiologic cross-sectional area

### *Statistical analysis*

To evaluate the correlation between the integrated EMG values and the analyzed muscle forces statistically, a simple regression analysis was performed in each muscle. The muscle force of the biceps was calculated as the sum of the forces of both the long and short heads. The regression functions were considered significant at $P < .05$.

## RESULTS

The results of the computer simulation are shown in Figure 6. The muscle forces and the reaction force were normalized and expressed as a percentage of body weight. The middle fiber of the deltoid demonstrated the largest force, with a peak value (27.5% of body weight) at 75° abduction, followed by the supraspinatus (10.9% of body weight), the anterior fiber of the deltoid (9.5% of body weight), and the infraspinatus (8.0% of body weight). These muscles acted continuously during the whole motion. On the other hand, the teres minor was active in the latter half of abduction, and the subscapularis acted only in the

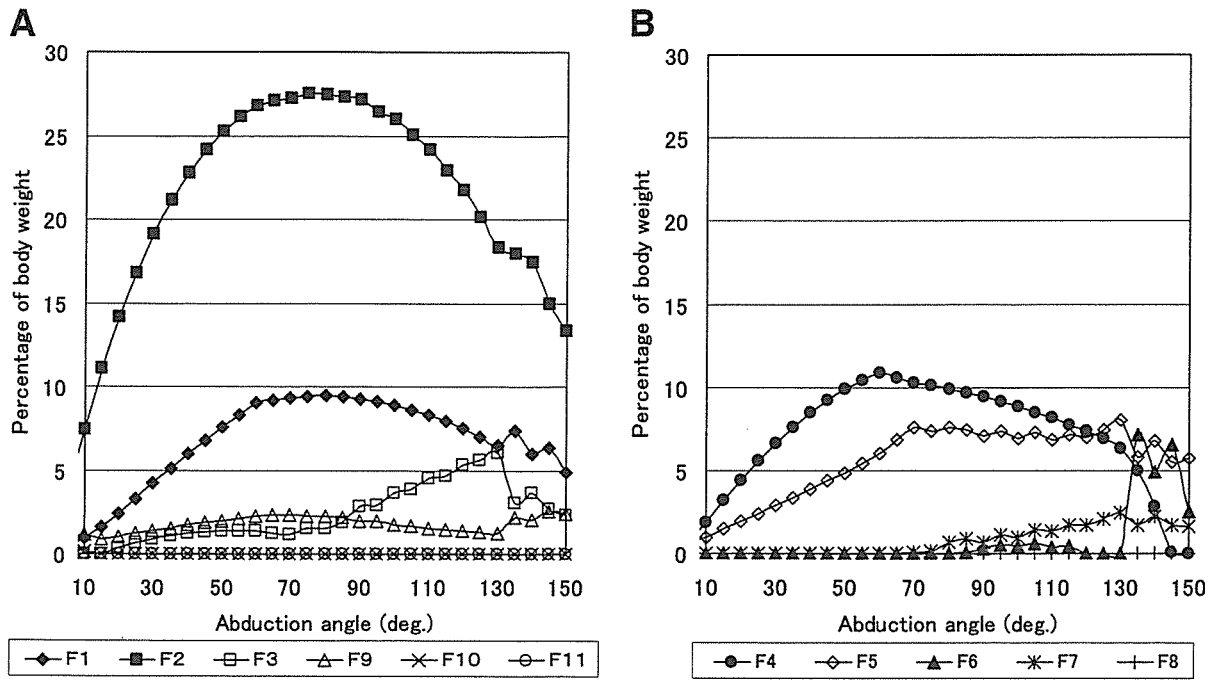


**Figure 6 A** and **B**, Relationship between muscle force and abduction angle obtained from computer simulation.

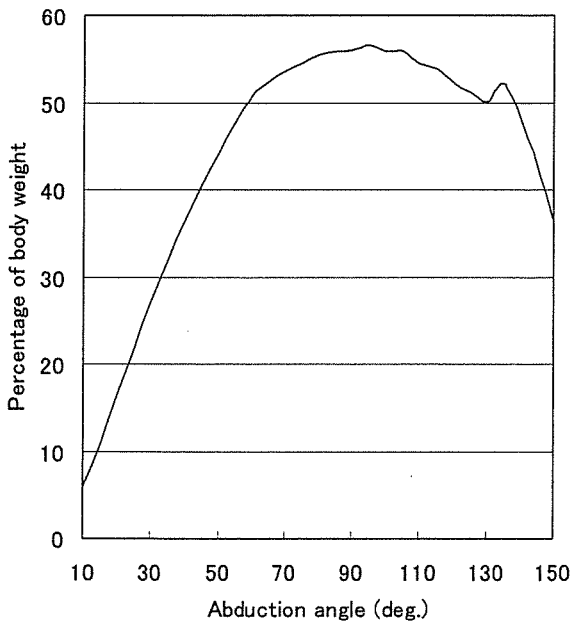


**Figure 7** Joint reaction force calculated from method.

last phase. The teres major and triceps demonstrated no muscle forces. The joint reaction force showed its maximum value of 56.5% of body weight at 95° abduction (Figure 7).

The optimal origin points of the 6 wide muscles (F1-F6) selected in each abduction angle changed as the shoulder joint abducted, as shown in Figure 8, which shows the relationship between the optimal point and the abduction angle in the supraspinatus and infraspinatus as examples.

The results of EMG are shown in Figure 9. The middle fiber of the deltoid demonstrated the largest value, followed by the supraspinatus, anterior fiber of the deltoid, and infraspinatus. These muscles showed gradual increases, whereas the analyzed forces peaked and then declined. In the subscapularis, on the other hand, the value increased in the last phase of abduction, as did the analyzed force.

The significant regression functions between the analyzed muscle forces and the integrated EMG values were obtained in all muscles except for the triceps and teres major, which showed no muscle forces in the analysis (Table II).

## DISCUSSION

In numerical muscle force analyses, a straight-line vector, a centroid line, or a bony contour line have been mainly used in muscle modeling.[1,4,5,7,11,16,17] However, modeling of a muscle originating from a wide area has been a problem, because it is unreasonable for a single fixed straight-line vector to represent the muscle and, moreover, the direction of the muscle action can change depending on the joint position. To solve this problem, Högfors et al[4] proposed dividing muscles with large attachment sites

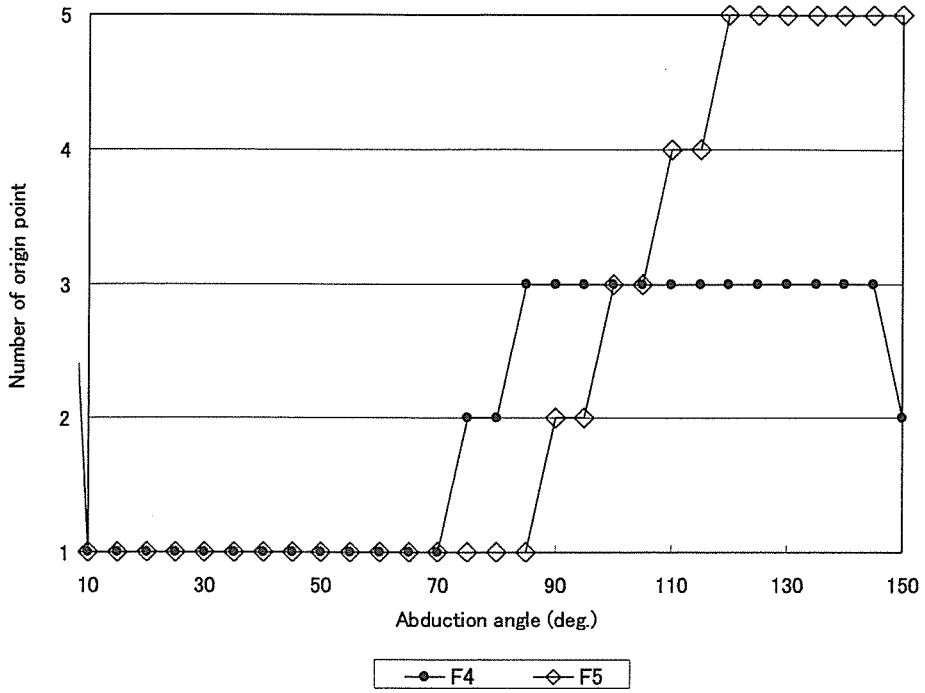


**Figure 8** The optimal origin points of the supraspinatus and infraspinatus selected in each abduction angle are indicated as an example.

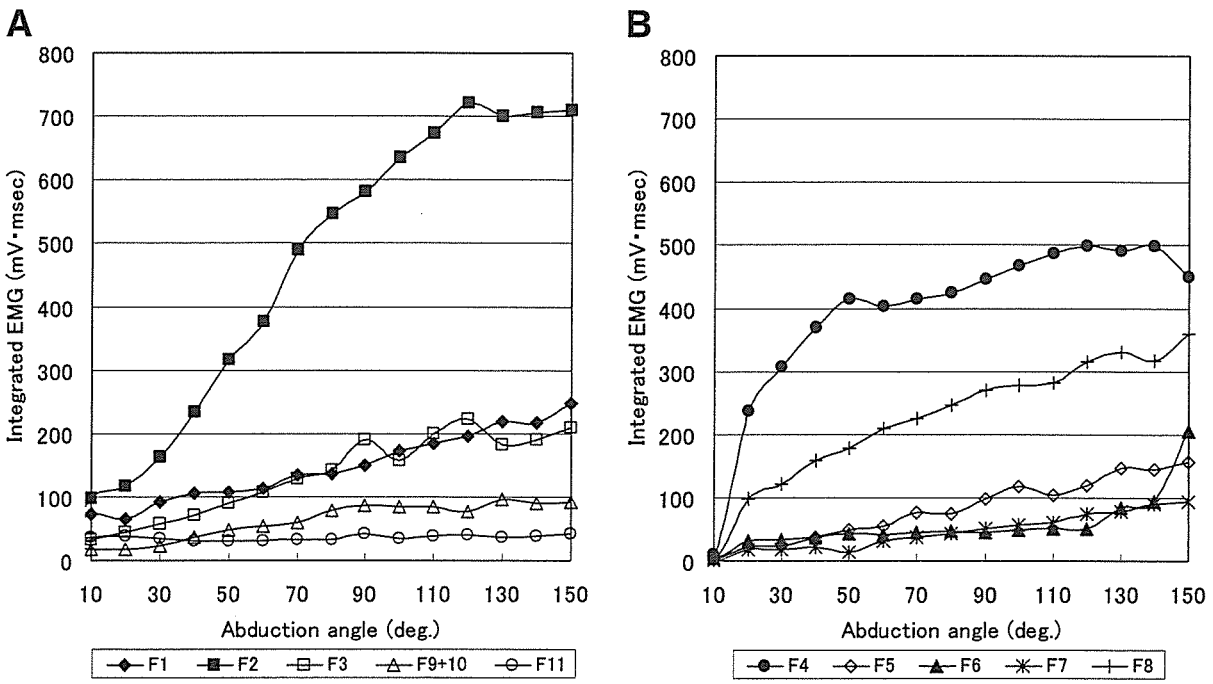


**Figure 9 A** and **B**, Integrated EMG values.

into several muscle lines of action. Karlsson and Peterson[7] calculated the shoulder muscle forces using the divided vector model and reported that some of the results were reasonable whereas others were not. How to determine the number of muscle lines of action is still controversial, although Van der Helm and

**Table 2** The regression functions between the analyzed muscle forces and the integrated EMG values

| Muscle | Regression function | P value | R |
|---|---|---|---|
| F1; Anterior fiber of deltoid | y = 57.94 x + 73.49 | 0.037 | 0.523 |
| F2; Middle fiber of deltoid | y = 84.79 x + 117.26 | 0.047 | 0.503 |
| F3; Posterior fiber of deltoid | y = 159.38 x + 58.57 | 0.000 | 0.848 |
| F4; Supraspinatus | y = 111.72 x + 231.86 | 0.037 | 0.525 |
| F5; Infraspinatus | y = 85.99 x − 9.96 | 0.000 | 0.805 |
| F6; Subscapularis | y = 110.60 x + 44.22 | 0.010 | 0.624 |
| F7; Teres minor | y = 158.65 x + 21.52 | 0.000 | 0.930 |
| F8; Teres major | unanalyzable | | |
| F9 + F10; Biceps | y = 142.58 x + 14.02 | 0.048 | 0.500 |
| F11; Triceps | unanalyzable | | |

EMG, electromyography

Veenbaas[16] reported that there is an appropriate number of muscle lines that represent a muscle force. In our study, we proposed a new method to determine the optimal origin point of muscles that originate from a wide area; the origin point was not predetermined but was defined in every joint position. The fact that the optimal origin point in each abduction angle shifted in all wide muscles in our study suggests that it is unreasonable for a fixed-line vector to represent these muscles at different moments of a motion. However, as the current model is preliminary, there are some aspects that should be considered for further development of the model. For the muscles in which not only the origin area but also the insertion area is wide, as in the serratus anterior, we also have to consider other options such as dividing the muscles into several parts. The optimal origin point was selected from only several points on the straight line in this study. In the next stage, the optimal point should be picked from any point on the 3-dimensional origin surface.

EMG has been used to validate the results of the analysis by comparing them qualitatively in previous studies.[1,7] However, it is known that EMG amplitude is length-dependent,[3,17] so EMG values cannot be directly compared among different muscles and often result in large amplitudes near full elevation angles, whereas the analyzed forces decrease. In this study, EMG values showed gradual increase, whereas analyzed values showed their peaks at the middle phase of the motion in some of the muscles. Despite that, the muscle forces and EMG values showed quantitative correlations. Therefore, although it is controversial to use EMG values as an indicator for validation because the EMG-force relationship is unknown for shoulder muscles,[17] as long as there is no other established method by which to validate the predicted muscle forces, we consider that EMG can be an indicator to validate (at least) the pattern of muscle forces.

In our study, the maximum joint reaction force was calculated to be 56.5% of body weight. In previous reports, the joint reaction force ranged from 44% to 92% of body weight.[6,7,12,13] Although the values cannot be compared directly because the method, condition, and assumption of each study vary greatly, our result is considered to be a comparable and reasonable value.

There are still some considerable limitations in this study. The model includes only the muscles that originate from the scapula. To simulate various conditions of a shoulder joint, a whole system including bone structures and muscles related to the thorax must be developed. This study is a static analysis with only the equilibrium conditions of force and moment. Therefore, the stiffness and time-dependent fatigue of muscles are not considered, nor are soft tissues such as joint capsules or ligaments that stabilize the glenohumeral joint.

Our model is capable of being applied to individual clinical patients to simulate their shoulder muscle activities, because anatomic data can be easily introduced from CT data. The simulation would provide useful information regarding how the other normal muscles work in a compensatory manner in pathologic conditions, such as tendon ruptures or muscle paralyses. It would also be possible to simulate surgical treatment, such as tendon or muscle transfers, to predict preoperatively the effects of surgical procedures and their influence on the other muscles.

In conclusion, we have developed a 3-dimensional shoulder biomechanical model using an original method of determining vectors of muscles originating from a wide area. The results of the numerical analysis were in correlation with the integrated EMG values, therefore allowing for the simulation of cooperative abduction muscle activities in vivo. We believe that this novel concept will provide a new approach in modeling a variety of muscles with a wide origin area and the possibility for more precise simulations of muscle activities in a living body.

We thank Dr Satoshi Yoshinari, Hokkaido Industrial Research Institute, for his previous work and help, as well as

the radiologic technologists at Sapporo Hokuyu Hospital for their help in collecting the CT data for this study.

**REFERENCES**

1. Crowninshield RD, Brand R. A physiologically based criterion of muscle force prediction in locomotion. J Biomech 1981;11:793-801.
2. Fujisawa H, Suenaga N, Minami A. Electromyographic study during isometric exercise of the shoulder in head-out water immersion. J Shoulder Elbow Surg 1998;7:491-4.
3. Heckathorne CW, Childress DS. Relationships of the surface electromyogram to the force, length, velocity, and contraction rate of the cineplastic human biceps. Am J Phys Med 1981;60:1-19.
4. Högfors C, Sigholm G, Herberts P. Biomechanical model of the human shoulder—I. Elements. J Biomech 1987;20:157-66.
5. Högfors C, Karlsson D, Peterson B. Structure and internal consistency of a shoulder model. J Biomech 1995;28:767-77.
6. Inman VT, Saunders JB, Abbott LC. Observations on the function of the shoulder joint. J Bone Joint Surg 1944;26:1-30.
7. Karlsson D, Peterson B. Towards a model for force predictions in the human shoulder. J Biomech 1992;25:189-99.
8. Kronberg M, Németh G, Broström LA. Muscle activity and coordination in the normal shoulder. An electromyographic study. Clin Orthop 1990:76-85.
9. McClure PW, Michener LA, Sennett BJ, Karduna AR. Direct 3-dimensional measurement of scapular kinematics during dynamic movements in vivo. J Shoulder Elbow Surg 2001;10:269-77.
10. Meek SG, Wood JE, Jacobsen SC. Model-based, multi-muscle EMG control of upper-extremity prostheses. In: Winters JM, Woo SL-Y, editors. Multiple muscle systems: biomechanics and movement organization. New York: Springer-Verlag; 1990. p. 360-76.
11. Niemi J, Nieminen H, Takala EP, Viikari-Juntura E. A static shoulder model based on a time-dependent criterion for load sharing between synergistic muscles. J Biomech 1996;29:451-60.
12. Parsons IM, Apreleva M, Fu FH, Woo SL. The effect of rotator cuff tears on reaction forces at the glenohumeral joint. J Orthop Res 2002;20:439-46.
13. Poppen NK, Walker PS. Forces at the glenohumeral joint in abduction. Clin Orthop 1978:165-70.
14. Sigholm G, Herberts P, Almström C, Kadefors R. Electromyographic analysis of shoulder muscle load. J Orthop Res 1984;1:379-86.
15. Suenaga N, Minami A, Fujisawa H. Electromyographic analysis of internal rotational motion of the shoulder in various arm positions. J Shoulder Elbow Surg 2003;12:501-5.
16. Van der Helm FCT, Veenbaas R. Modelling the mechanical effect of muscles with large attachment sites: application to the shoulder mechanism. J Biomech 1991;24:1151-63.
17. van der Helm FCT. Analysis of the kinematic and dynamic behavior of the shoulder mechanism. J Biomech 1994;27:527-50.

*Connective Tissue Research*, 47:141–148, 2006

ISSN: 0300-8207 print / 1521-0456 online
DOI: 10.1080/03008200600685459

Taylor & Francis
Taylor & Francis Group



# Extracellular Matrix Modulates Expression of Cell-Surface Proteoglycan Genes in Fibroblasts

**N. Sawaguchi, T. Majima, N. Iwasaki, T. Funakoshi, K. Shimode, T. Onodera, and A. Minami**

*Department of Orthopedic Surgery and Frontier Research Center for Post-Genomic Science and Technology, Hokkaido University School of Medicine, Sapporo, Japan*

**Cell-surface proteoglycans are involved in many functions, including interactions with components of the extracellular microenvironment. They also act as coreceptors that bind and modify the actions of various growth factors, cytokines, and the extracellular matrix (ECM). This study investigated the regulation by the ECM of the expression of cell-surface proteoglycans (CD44, syndecan-1–4, betaglycan, glypican-1). We examined the changes in the expression levels of cell-surface proteoglycan genes in intact tendon, monolayer culture, and under various culture conditions. There was a significant increase in the expression of CD44 and syndecan-4 mRNAs during cell isolation from the tendon. With the switch to a 3D culture environment, there was a significant increase in the expression of CD44 at each passage point relative to its expression in 2D at those passage points. Syndecan-4 mRNA also increased steadily at each passage point in 3D culture environment. This influence on cell surface proteoglycans gene expression may indicate that collagen gel culture mimics in vivo tendon environment. This study provides further insight into the regulation of cell-surface proteoglycans in ligament and tendon fibroblasts by the ECM and 3D culture conditions.**

**Keywords:** CD44, Collagen, Fibroblast, Gel, HSPG, Hyaluronan

## INTRODUCTION

Cell-surface proteoglycans are involved in various functions, including interactions with components of the extracellular microenvironment. They also act as coreceptors that bind and modify the actions of various cell adhesion molecules, growth factors, and cytokines [1]. The structural multiplicity of the core proteins and glycosaminoglycan moieties, as well as their highly regulated patterns of expression, allow distinct functions for each cell-surface proteoglycan [2, 3]. This suggests that the responses of cell-surface proteoglycans to various biological effecter molecules are selective and cell-type specific.

Received 13 September 2005; accepted 5 March 2006.

Address correspondence to Naohiro Sawaguchi, MD, Department of Orthopaedic Surgery, Hokkaido University School of Medicine, North 15 West 7, Kita-Ku, Sapporo 060-8638, Japan. E-mail: sawa717@med.hokudai.ac.jp

In living organisms, the authentic substrate for most cells is the extracellular matrix (ECM) that adheres to cells via integrins, which are membrane-spanning heterodimeric receptors. Through this adhesion, the ECM transduces physiological signals to the cells, which regulate cell growth, cell proliferation, cell differentiation, and matrix remodeling [4]. Therefore, the interactions between cells and the ECM play a critical role in living tissue development, repair, and regeneration. In a tissue-engineering technique, tissue regeneration is achieved by culturing isolated cells on scaffolds of biocompatible and biodegradable materials onto which the cells are seeded. Many studies have shown the importance of selecting the appropriate biomaterials as scaffolds for cell adhesion and to support proliferation [5–10]. The interactions between scaffold materials and isolated cultured cells should closely mimic the natural environment of the tissue-specific ECM to achieve successful tissue regeneration [6]. However, few reports have investigated cell-matrix interaction in the context of tendon tissue engineering.

The response of cells to both pericellular matrix molecules and soluble stimuli such as growth factors and cytokines can be modulated by proteoglycans. The CD44 (hyaluronan receptor), betaglycan (transforming growth factor [TGF]-$\beta$ type III receptor), syndecan (transmembrane heparan sulfate proteoglycan), and glypican (glycosylphosphatidyl inositol [GPI]-anchored heparan sulfate proteoglycan) families [1, 11–15] are well-known cell-surface proteoglycans. However, little is known about the changes in the expression of these proteoglycans during growth in culture. As mentioned, elucidation of this point should lead to the development of an ideal scaffold material that simulates the natural environment of the tissue-specific ECM.

Hyaluronan (HA) is a high-molecular-weight polymer of disaccharide units comprised of glucuronic acid and acetylglucosamine. It is produced by cells at different rates and probably with different purposes over a lifetime. The biological role of HA must be important because it is one of the most ancient and well-represented glycosaminoglycans in living organisms. We originally developed a novel chitosan-based HA

hybrid polymer fiber as a scaffold material for ligament/tendon tissue engineering [16]. Our results previous studies have shown that HA enhances the cellular activities of fibroblasts, including their adhesivity, proliferation, and ECM synthesis. Although HA has these superior biological properties, its influence on cells has not been clarified. An understanding of how matrix contacts are assembled and coordinated by cells could open up new strategies to manipulate cell locomotion, matrix assembly, or cell interactions in tissue engineering applications [17].

The hypothesis of our study was that the expression of cell-surface proteoglycans is altered by culture conditions. To test this hypothesis, we quantified the expression of cell-surface proteoglycans on fibroblasts under various culture conditions in vitro. The first objective was to evaluate the changes in the expression of cell-surface proteoglycans with passages of a monolayer fibroblast culture. The second objective was to clarify the effects of HA, a major component of tissue ECMs, and of the dimensionality of fibroblast culture on the expression of proteoglycans. Our results presented here provide valuable information for the development of scaffold materials and for tendon and ligament tissue engineering.

## MATERIALS AND METHODS

### Cell Isolation and Monolayer Culture

Fibroblasts were isolated from the patella and Achilles tendons of adult male Wistar rats weighing 280–320 g. Cells were collected from the tendon by digestion with 0.25% collagenase (Invitrogen Corp., Carlsbad, CA, USA) and 0.25% trypsin–EDTA (Invitrogen). These cells isolated directly from tissue were designated passage 0 (P0). For culture, Dulbecco's modified Eagle's medium (Sigma Chemical, St Louis, MO, USA) was used with 10% fetal bovine serum (Invitrogen), 1% antibiotics (penicillin–streptomycin–fungizone 100 × concentrate, BioWhittaker, Walkersville, MD, USA). The isolated cells were seeded onto polystyrene culture dishes (well diameter 60 mm; Corning, Corning, NY, USA) at 10000 cells/cm$^2$ and dishes coated with pepsin-solbilized type I collagen (3 mg/ml, cell matrix type I-P; Nitta Gelatin, Tokyo, Japan) as instructed in the manual from Nitta Gelatin.

To evaluate the effects of HA on the expression of proteoglycans, the culture dishes containing type I collagen were coated with HA (MW = 210 kDa; Denkikagaku Kogyo, Tokyo, Japan) at 0.1% final concentration. Fibroblast cultures were incubated in a humidified incubator at 37°C in 5% $CO_2$ and the medium was replaced twice a week. At confluence, cultures were designated P1. Subsequent passages (P2 and P3) were achieved with trypsinization and division of cells at a 1:3 ratio.

### Three-Dimensional (3D) Culture

In the second experiment examining 3D cultures, six-well flat-bottom culture dishes (well diameter 35 mm; Becton Dickson, Franklin Lakes, NJ, USA) were filled with type I collagen gel (Nitta Gelatin) or type I collagen gel plus 210-kDa HA at final 0.1% concentration. The collagen gels were prepared as instructed in the manual from Nitta Gelatin. Briefly, acid-solubilized porcine collagen type I (3 mg/ml, cell matrix type I-A; Nitta Gelatin), 5 × Dulbecco's modified Eagle's medium, reconstitution buffer (0.05 M NaOH, 0.26 M $NaHCO_3$, and 200 mM HEPES pH 7.3) were mixed in a ratio of 7:2:1 in an ice bath. Then 1 ml of this solution was placed on a 6-well culture dish as a basal layer. After polymerization at 37°C for 30 min, 2 ml of same collagen solution but containing $5 \times 10^4$ cells/ml was overlaid on the basal collagen layer, and again allowed to polymerize at 37°C for 30 min. Then 2 ml of DMEM was added to the top of the collagen gel, and cells were cultured. Culture dishes were incubated at 37°C in 5% $CO_2$, until the cells appeared confluent as observed by light microscopy. These cultures were designated P1. Subsequent passages (P2 and P3) were achieved with digestion with collagenase and trypsin–EDTA, and division of cells at a 1:3 ratio.

### RNA Extraction

Total RNA was extracted from the tendon and cultured fibroblasts at each passage (P0, P1, P2, and P3) using standard TRIzol reagent (Invitrogen) according to the manufacturer's instructions. Tendons were weighed and snap-frozen in liquid nitrogen before RNA extraction. After DNase digestion, RNA samples were passed through RNeasy MinElute Cleanup Kit (Qiagen, Valencia, CA, USA) according to the manufacturer's instructions. The RNA concentration and the quality of all samples were determined spectrophotometrically.

### RT–PCR

For cDNA synthesis, 1 $\mu$g of RNA was reverse-transcribed using random hexamer primers (Promega, Madison, WI, USA) and Improm-II reverse transcriptase (Promega) according to the supplier's instructions. Real-time PCR was performed using OPTICON II (Bio-Rad Laboratories, Hercules, CA, USA) in a 20-$\mu$L reaction volume. Signals were detected using the SYBR Green qPCR Kit (Finzymes, Espoo, Finland) with gene-specific primers designed using OLIGO (Molecular Biology Insights, Cascade, CO, USA) (Table 1). Real-time analysis involved a 15-min denaturing step, followed by 40 cycles of 10 sec at 94°C, 20 sec at 56°C, and 30 sec at 72°C. Fluorescence measurements were made at every 72°C cycle to provide quantitative real-time analysis of the gene analyzed. Real-time PCR has become increasingly common and gives quantitative values for the expression of any gene of interest [18, 19].

A major advantage to this technique is its provision of a cycle-by-cycle view of gene amplification for a sample group. The take-off cycle for each gene is recorded and used in a relative abundance equation to quantify the gene expression of the sample. The melting temperature profiles of amplicons were determined to show the specificity of the amplification.

TABLE 1
Sequences of primers

| Gene | Sequence | GenBank Accession No. |
|---|---|---|
| CD44 | 5′-CCGTTACGCAGGTGTATTCC-3′ | U96139 |
| | 5′-TGTTGAAAGCCTCGCAGAG-3′ | |
| SDC-1 | 5′-CCTACCGCTGTGCCGTCT-3′ | M81785 |
| | 5′-TGCACCCAAGCTTCTAGCAG-3′ | |
| SDC-2 | 5′-TGTTCAAGCGGACGGAGGT-3′ | NM_013082 |
| | 5′-TTGCGTTCTCCAAGGTCGTA-3′ | |
| SDC-3 | 5′-CTTGGCCTCCACGACAAT-3′ | U52825 |
| | 5′-GCACCTCCTTCCGCTCTAGT-3′ | |
| SDC-4 | 5′-GATTGTGGGCGGCGTAG-3′ | NM_012649 |
| | 5′-CTTGCCCAAGTCGTAACTGC-3′ | |
| Betaglycan | 5′-GCCGCCGAAGGTTGTG-3′ | M77809 |
| | 5′-CTGGAAAGCGCTGTAAGGGT-3′ | |
| GPC-1 | 5′-GGTGTGGCCAGTGACGTAG-3′ | NM_030828 |
| | 5′-TTGAGCACATTTCGGCAATA-3′ | |
| GPC-3 | 5′-GAGCTCGTGAACGGCATGTA-3′ | NM_012774 |
| | 5′-GGAGTGGGCGCACAACT-3′ | |
| Gapd | 5′-GCTGGTCATCAACGGGAAA-3′ | X02231 |
| | 5′-ACGCCAGTAGACTCCACGAC-3′ | |

Gapd = glyceraldehyde phosphate dehydrogenase gene.

To quantify gene expression, the comparative Ct method was used. The difference between the mean ΔCt value of the gene of interest and that of the housekeeping gene (GAPD) is denoted (Δ–Ct) and the difference between Δ–Ct and the Ct value of the calibrator sample is Δ–Δ–Ct. $Log_2$(Δ–Δ–Ct) is the relative quantitative value for the expression of a gene when the expression value for that gene in intact tendon is deemed to be 1.

A one-way analysis of variance (ANOVA) was used to evaluate the effects of passage on culture conditions and with or without HA in each gene expression (Δ–Ct). For the assessment the effect of passage and culture conditions, and of passage with or without HA, a two-way ANOVA was performed, and then a Tukey-Kramer analysis was applied to determine the significance of difference. The significance limit was taken at $p = 0.05$.

## RESULTS

### Expression Levels of Proteoglycans

Results are reported as the relative value for each gene in culture compared with level of mRNA for that gene in the intact tendon tissue (Figure 1). There were significant increases in the expression of CD44 ($p < 0.01$) and syndecan-4 ($p < 0.01$) during the proteolytic digestion of the tendon. However, the mRNAs of the other proteoglycans (syndecan-1, -2, betaglycan, glypican-1) decreased significantly ($p < 0.05$) at P0. During

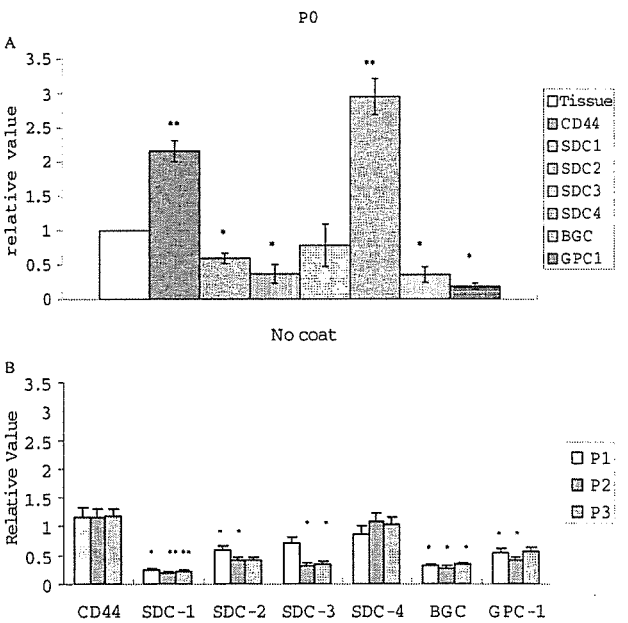


FIG. 1. Quantitative expression of proteoglycan genes is given as the fold difference ($2^{-\Delta\Delta Ct} \pm SD$) between tissue and cell samples ($n = 3$–5). (A) P0. (B) Cells cultured on noncoated plates. SDC = syndecan, BGC = betaglycan, GPC = glypican. Glypican-3 mRNA was below the detection limit of real-time RT–PCR in each sample. $^*p < 0.05$, $^{**}p < 0.01$.

subsequent culture on noncoated plates, there was no significant change in CD44 and syndecan-4 expression compared with their expression in tissue. However, the expression of the other proteoglycans significantly decreased at each passage point ($p < 0.05$).

### Effects of ECM-Coated Plates

The mRNA expressions of the proteoglycans related to collagen coat and passage are shown in Figure 2 and Table 2. There was no significant difference in the expression of CD44 and syndecan-4 at each passage when cultured on noncoated plates or on type I collagen-coated plates. The expression of syndecan-1, -2, and glypican-1 were increased significantly at

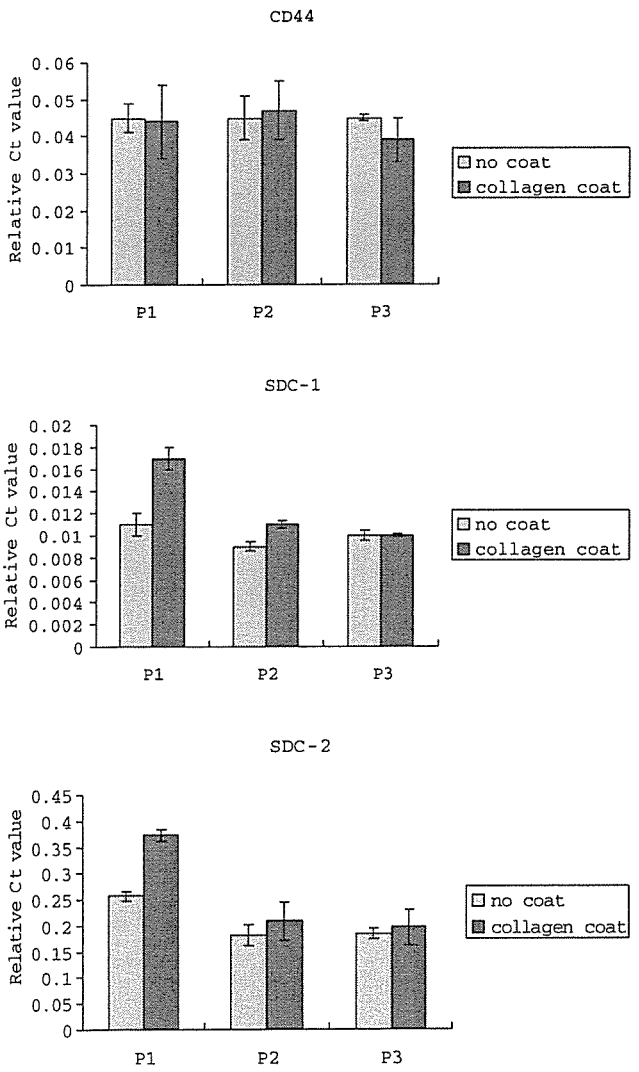


FIG. 2. The mRNA expressions of the proteoglycans related to collagen coat and passage in 2D culture is given as the relative Ct value ($2^{-\Delta Ct} \pm SD$) ($n = 3$–5). SDC = syndecan; BGC = betaglycan; GPC = glypican.

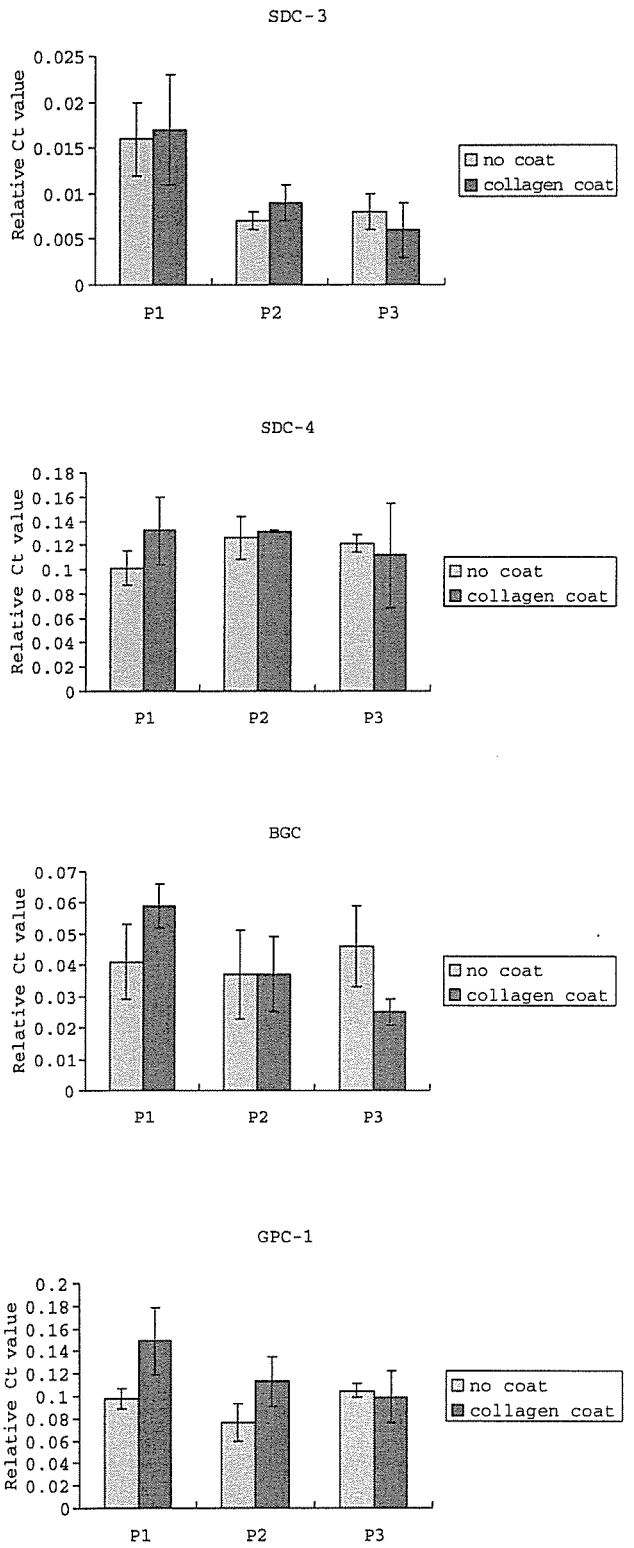


FIG. 2. (Continued)

TABLE 2
mRNA expressions of the proteoglycans (PGs) related to collagen coat and passage[a]

| | Passage | | | | Passage | | |
|---|---|---|---|---|---|---|---|
| | P1 | P2 | P3 | | P1 | P2 | P3 |
| | No coat | | | | Collagen coat | | |
| CD44 | .0452 ± .0303 | .0452 ± .0075 | .0452 ± .0075 | CD44 | .0445 ± .0061 | .0468 ± .0108 | .0391 ± .0010 |
| SDC-1[b] | .0110 ± .0016[c] | .0092 ± .0009[c] | .0104 ± .0010 | SDC-1[b] | .0167 ± .0025[c,d,e] | .0112 ± .0005[c,d] | .0098 ± .0002[e] |
| SDC-2 | .2566 ± .0182[c,d,e] | .1809 ± .0393[d] | .1851 ± .0209[e] | SDC-2 | .3733 ± .0210[c,d,e] | .2085 ± .0633[d] | .1956 ± .0612[e] |
| SDC-3 | .0156 ± .0046[d] | .0073 ± .0015[d,e] | .0076 ± .0021[e] | SDC-3 | .0166 ± .0065[e] | .0090 ± .0025 | .0056 ± 0026[e] |
| SDC-4 | .1012 ± .0288 | .1257 ± .0358 | .1213 ± .0146 | SDC-4 | .1321 ± .0277 | .1306 ± .0012 | .1117 ± .0432 |
| BGC | .0411 ± .0123 | .0370 ± .0145 | .0457 ± .0132[c] | BGC | .0587 ± .0071[d,e] | .0369 ± .0067[d] | .0250 ± .0036[c,e] |
| GPC-1[b] | .0976 ± .0093[c] | .0764 ± .0165[f] | .1055 ± .0063[f] | GPC-1[b] | .1149 ± .0303[c] | .1127 ± .0219 | .0994 ± .0231 |

[a]Mean ± SE; $n = 4$ for each passage. SDC = syndecan, BGC = betaglycan, GPC = glypican.
[b]Two-way analysis of variance demonstrated significant difference with respect to collagen coat ($p < 0.05$) and passage ($p < .005$). There was significant interaction between collagen coat and passage.
[c]Significantly different with collagen coat to each PG at same passage (one-way analysis of variance).
[d]Significantly different with passage (P1 vs. P2) to each PG (one-way analysis of variance).
[e]Significantly different with passage (P1 vs. P3) to each PG (one-way analysis of variance).
[f]Significantly different with passage (P2 vs. P3) to each PG (one-way analysis of variance).

P1 when cultured on type I collagen-coated plates, and then their expression declined steadily. There was no significant difference in the expression of syndecan-1, -2, and glypican-1 between the noncoated plates and the type I-coated plates culture at P3. On noncoated plates and on type I collagen-coated plates, syndecan-3 mRNA expression was decreased on each passage. On noncoated plates, betaglycan mRNA showed no change with passage, whereas that on type I collagen-coated plates declined steadily. The mRNA expressions of the PGs related to dimension with or without HA are shown in Figure 3 and Table 3. With the addition of HA to the collagen, syndecan-2 mRNA increased at P1, after which its expression declined steadily. Syndecan-1 and betaglycan mRNAs showed no change at each passage, whereas that on type I collagen-coated plates declined steadily. CD44 mRNA increased at P3 in collagen + HA-coated plate culture.

### Effect of Culture Dimensions

With the switch to a 3D culture environment, there was a significant increase in the expression of CD44 at each passage point relative to its expression in 2D at those passage points. Furthermore, the expression of CD44 increased steadily under 3D conditions. Syndecan-4 mRNA also increased steadily at each passage point. There was a significant increase in its expression in 3D culture relative to its expression in 2D culture. There was a significant increase in the expression of syndecan-2 at each passage point relative to its expression in 2D at those passage points. Betaglycan and symdecan-1 mRNA showed no change by passage, while that on type I collagen-coated plates declined steadily. With the addition of HA to collagen gels, the expression of syndecan-4 increased significantly at P1, the expression of betaglycan increased significantly at P1 and P2 while that decreased at P3. There was no significant difference in the expression of CD44 at each passage. Syndecan-3, and glypican-1 showed patterns of expression similar to those observed under 2D culture conditions.

## DISCUSSION

In the present study, we clarified the change in the expression of fibroblast cell-surface proteoglycan genes, which is modulated by growth factors and cytokines, during the isolation and culture of fibroblasts. During cell isolation and monolayer culture, the expression of syndecan-1, -2, and -3, betaglycan, and glypican-1 mRNAs decreased steadily. In contrast, during the retrieval of cells from the tendon, there was a dramatic increase in the expression of mRNAs for CD44 and syndecan-4, which are closely related to cell adhesion. Syndecan-4 is the only syndecan that is a widespread component of focal adhesions [11]. CD44 mediates HA-dependent cell adhesion, which has been observed in a number of different cell types including fibroblasts [20]. Hyaluronan constitutes 22% of the glycosaminoglycans in the patella tendon [21]. These findings indicate that HA is an important macromolecule on ligament and tendon fibroblasts. Syndecan-2 is the major syndecan in fibroblasts and regulates TGF-$\beta$ signaling [22]. Syndecan-2 interacts with matrix proteins such as laminin [23] and fibronectin [24]. Betaglycan, also a type III TGF-$\beta$ receptor, syndecan-2, and betaglycan gene expression were suppressed in monolayer culture.

Switching fibroblasts from monolayer to 3D collagen culture allowed them to take on functional properties that more closely resemble those of fibroblasts *in vivo* [25, 26]. In the present study, the switch to 3D culture induced a dramatic increase in

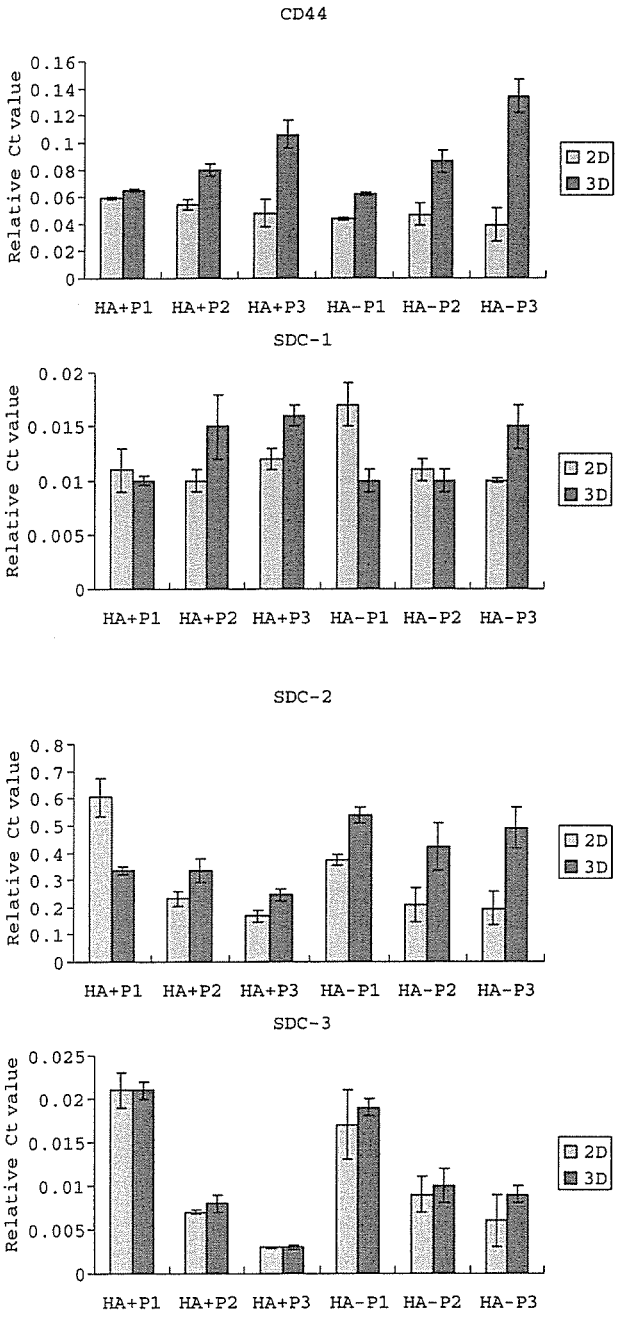


FIG. 3. The mRNA expressions of the proteoglycans related to dimension with or without hyaluronan (HA) are given as the relative Ct value ($2^{-\Delta Ct} \pm SD$) ($n = 3$–5). HA+ = with addition of HA to the collagen; HA− = without addition of HA to the collagen; SDC = syndecan; BGC = betaglycan; GPC = glypican.

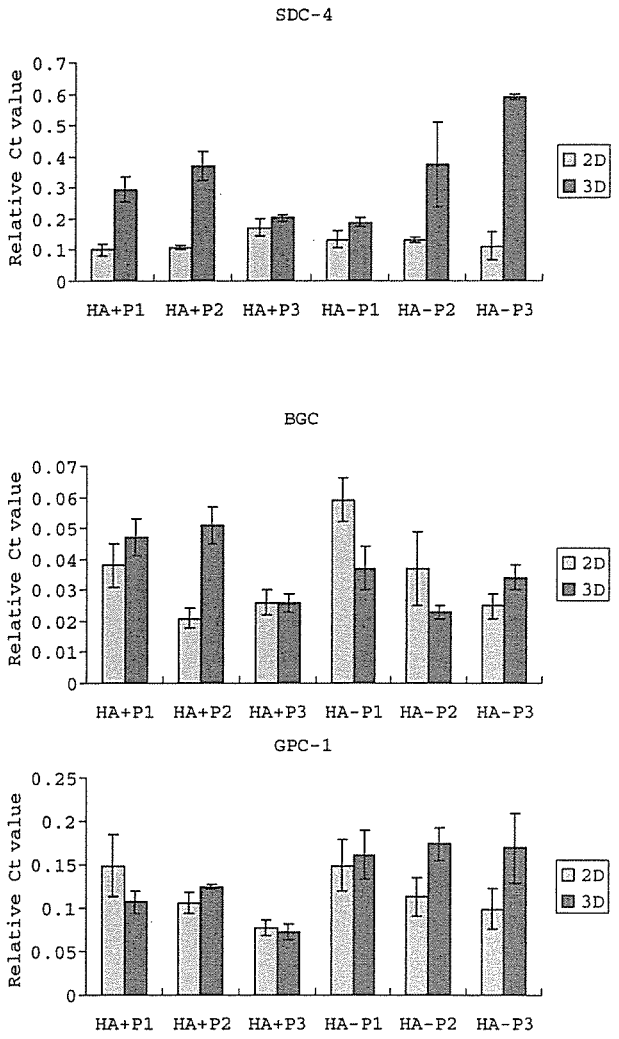


FIG. 3. (Continued)

the expression of syndecan-4. Dermatan sulfate proteoglycans and glycosaminoglycan synthesis are induced in fibroblasts by transfer to a 3D extracellular environment [27]. These findings underscore the importance of the extracellular environment in influencing cell behavior. In the previous study, much emphasis was placed on medium composition, ambient gas mixture, and incubation in cell culture to better simulate in vivo conditions. Less consideration has been given to the potential influence of culture architecture on cell behavior. An obvious difference relative to the normal environment is the loss of contact with the surrounding ECM. Change in cell-surface proteoglycan gene expression may indicate that collagen gel culture mimics the *in vivo* tendon environment.

With the addition of HA to the collagen matrix, significant differences were observed at P3 in the expression of

TABLE 3
mRNA expressions of the proteoglycans (PGs) related to dimension, passage, and hyaluronan (HA)[a]

| | Passage | | | | Passage | | |
|---|---|---|---|---|---|---|---|
| | P1 | P2 | P3 | | P1 | P2 | P3 |
| | 2D (HA−) | | | | 3D (HA−) | | |
| CD44[b] | .0445 ± .0061[c] | .0468 ± .0108[c] | .0391 ± .0010[c,g] | CD44[b] | .0623 ± .0026[c,e] | .0860 ± .0130[c,f] | .1345 ± .0214[c,e,f] |
| SDC-1[h] | .0167 ± .0025[c,d,e,g] | .0122 ± .0005[d] | .0097 ± .0002[c,e,g] | SDC-1 | .0096 ± .0009[c,e] | .0099 ± .0012[f] | .0154 ± .0018[c,e,f] |
| SDC- 2[h] | .3733 ± .0210[c,d,e,g] | .2085 ± .0633[c,d] | .1956 ± .0612[c,e] | SDC-2 | .5385 ± .0282[c,g] | .4229 ± .0880[c] | .4905 ± .0761[c,g] |
| SDC-3 | .0166 ± .0065[e] | .0090 ± .0025 | .0056 ± .0026[e] | SDC-3[h] | .0187 ± .0009[d,e] | .0103 ± .0019[d] | .0086 ± .0014[e,g] |
| SDC-4[b] | .1321 ± .0277[c] | .1306 ± .0012[c,g] | .1117 ± .0432[c] | SDC-4[b,h] | .1884 ± .0161[c,e,g] | .3717 ± .1347[c,f] | .5896 ± .0104[c,e,f,g] |
| BGC[b,h] | .0587 ± .0071[c,d,e,g] | .0369 ± .0067[d] | .0250 ± .0036[c,e] | BGC[b,h] | .0366 ± .0074[c,d] | .0227 ± .0025[d,g] | .0340 ± .0034[c,g] |
| GPC-1 | .1149 ± .0303 | .1127 ± .0219[c] | .0994 ± .0231 | GPC-1 | .1612 ± .0278[g] | .1745 ± .0186[c,g] | .1688 ± .0414[g] |
| | 2D (HA+) | | | | 3D (HA+) | | |
| CD44 | .0586 ± .0139 | .0538 ± .0126[c] | .0485 ± .0028[c,g] | CD44 | .0651 ± .0018[e] | .0802 ± .0065[c] | .1057 ± .0177[c,e] |
| SDC-1[b,h] | .0110 ± .0024[g] | .0099 ± .0009 | .0118 ± .0009[c,g] | SDC-1[b] | .0103 ± .0004[e] | .0146 ± .0036 | .0164 ± .0010[c,e] |
| SDC-2[h] | .6044 ± .0693[c,d,e,g] | .2318 ± .0262[c,d] | .1683 ± .0206[c,e] | SDC-2 | .3443 ± .0162[c,e,f,g] | .3437 ± .0422[c,f] | .2445 ± .0196[c,e,g] |
| SDC-3 | .0213 ± .0022[d,e,f] | .0067 ± .0002[c,d,f] | .0029 ± .0001[c,e,f] | SDC-3[h] | .0212 ± .0013[d,e,f] | .0085 ± .0007[c,d,f] | .0034 ± .0002[c,d,f,g] |
| SDC-4[b] | .1003 ± .0191[c,e,f] | .1081 ± .0082[c,f,g] | .1713 ± .0275[e] | SDC-4[b,h] | .2940 ± .0411[c,e,f,g] | .3685 ± .0463[c,f] | .2012 ± .0094[e,g] |
| BGC[b,h] | .0380 ± .0071[d,g] | .0214 ± .0032[c,d] | .0257 ± .0045 | BGC[b,h] | .0467 ± .0058[e,f] | .0514 ± .0058[c,f,g] | .0261 ± .0028[e,g] |
| GPC-1 | .1487 ± .0368[e] | .1062 ± .0116 | .0770 ± .0092[e] | GPC-1 | .1069 ± .0135[e,f,g] | .1250 ± .001 9[f,g] | .0728 ± .0091[e,g] |

[a]Mean ± SD; $n = 3$–4 for each passage. SDC = syndecan, BGC = betaglycan, GPC = glypican.

[b]Two-way analysis of variance demonstrated significant difference with respect to dimension ($p < 0.05$) and passage ($p < 0.05$). There was significant interaction between dimension and passage.

[c]Significantly different with dimension to each PG at same passage (one-way analysis of variance).

[d]Significantly different with passage (P1 vs. P2) to each PG (one-way analysis of variance).

[e]Significantly different with passage (P1 vs. P3) to each PG (one-way analysis of variance).

[f]Significantly different with passage (P2 vs. P3) to each PG (one-way analysis of variance).

[g]Significantly different with HA to each PGs at same passage (one-way analysis of variance).

[h]Two-way analysis of variance demonstrated significant difference with respect to HA ($p < 0.05$) and passage ($p < .05$). There was significant interaction between HA and passage.

CD44 in monolayer culture. Syndecan-2 mRNA increased at P1, after which its expression declined steadily. Syndecan-1 and betaglycan mRNAs showed no change at each passage, while that on type I collagen-coated plates declined steadily. Syndecan-4 mRNA increased significantly at P1, betaglycan mRNA increased significantly at P1 and P2 while it decreased at P3 in 3D culture. These findings indicate that HA affects the behavior of cells, and they are consistent with data suggesting that HA mediates cell-matrix interactions, as has been suggested for chondrocytes [28]. In recent studies, HA enhanced the contraction of collagen by smooth muscle cells and adventitial fibroblasts [29], but did not affect gel retraction by human dermal fibroblasts [30]. These data suggest that extracellular HA has different effects on different cell types.

The effect of HA on cellular adhesivity still is controversial. Several studies have demonstrated the highly cellular adhesivity of HA [31–35]. On the other hand, Zimmerman et al. [36] have shown that excess HA on a substrate strongly inhibits cell adhesion. Huang-Lee et al. [32] demonstrated that high concentrations of HA act as a barrier that interrupts the direct communication between fibroblasts and the ECM.

Therefore, in the present study, we investigated the effects of adding 0.1% HA to type I collagen. We did not determine the optimal concentration of HA that enhances cell activity. However, our previous studies showed that low concentrations of HA enhance the cellular activities of tendon fibroblasts, including their adhesivity, proliferation, and ECM synthesis [16].

## CONCLUSION

On the basis of this work, changes in the levels of cell-surface proteoglycan mRNAs appear to reflect the variability in the responsiveness of individual cell-surface proteoglycan genes to different ECM molecules. This provides one mechanism for the regulation of cell-surface proteoglycan production. Growth factors and cytokines modulate the expression of cell-surface proteoglycan genes [37]. The present study provides further insight into the regulation of cell-surface proteoglycans on ligament and tendon fibroblasts by the ECM and 3D culture condition. Their independently and selectively regulated expression constitutes a possible mechanism that renders cells differentially sensitive to the ECM in the repair and regeneration of ligament tissues.

## ACKNOWLEDGMENTS

This work was supported by a Grant-in-Aid for Science Research from the Ministry of Education, Culture, Sports, Science and Technology of Japan (B-1439044), a Grant-in-Aid for New Energy and Industrial Technology Development Organization (03A04002a), and the Akiyama Foundation.

## REFERENCES

1. Bernfield, M., Gotte, M., Park, P.W., Reizes, O., Fitzgerald, M.L., Lincecum, J., and Zako, M. (1999). Functions of cell surface heparan sulfate proteoglycans. *Annu. Rev. Biochem.*, 68, 729–777.
2. Cizmeci-Smith, G., Langan, E., Youkey, J., Showalter, L.J., and Carey, D.J. (1997). Syndecan-4 is a primary-response gene induced by basic fibroblast growth factor and arterial injury in vascular smooth muscle cells. *Arterioscler. Thromb. Vasc. Biol.*, 17, 172–180.
3. Cizmeci-Smith, G., Stahl, R.C., Showalter, L.J., and Carey, D.J. (1993). Differential expression of transmembrane proteoglycans in vascular smooth muscle cells. *J. Biol. Chem.*, 268, 18740–18747.
4. Hynes, R.O. (1999). Cell adhesion: old and new questions. *Trends Cell Biol.*, 9, M33–M37.
5. Jackson, D.W., Simon, T.M., Lowery, W., and Gendler, E. (1996). Biologic remodeling after anterior cruciate ligament reconstruction using a collagen matrix derived from demineralized bone. An experimental study in the goat model. *Am. J. Sports Med.*, 24, 405–414.
6. Lu, H.H., Jr., Cooper, J.A., Manuel, S., Freeman, J.W., Attawia, M.A., Ko, F.K., and Laurencin, C.T. (2005). Anterior cruciate ligament regeneration using braided biodegradable scaffolds: in vitro optimization studies. *Biomaterials*, 26, 4805–4816.
7. Jackson, D.W., Heinrich, J.T., and Simon, T.M. (1994). Biologic and synthetic implants to replace the anterior cruciate ligament. *Arthroscopy*, 10, 442–452.
8. Dunn, M.G., Liesch, J.B., Tiku, M.L., and Zawadsky, J.P. (1995). Development of fibroblast-seeded ligament analogs for ACL reconstruction. *J. Biomed. Mater. Res.*, 29, 1363–1371.
9. Altman, G.H., Horan, R.L., Lu, H.H., Moreau, J., Martin, I., Richmond, J.C., and Kaplan, D.L. (2002). Silk matrix for tissue engineered anterior cruciate ligaments. *Biomaterials*, 23, 4131–4141.
10. Bourke, S.L., Kohn, J., and Dunn, M.G. (2004). Preliminary development of a novel resorbable synthetic polymer fiber scaffold for anterior cruciate ligament reconstruction. *Tis. Engg.*, 10, 43–52.
11. Woods, A. (2001). Syndecans: transmembrane modulators of adhesion and matrix assembly. *J. Clin. Invest.*, 107, 935–941.
12. Filmus, J., and Selleck, S.B. (2001). Glypicans: proteoglycans with a surprise. *J. Clin. Invest.*, 108, 497–501.
13. Fransson, L.A. (2003). Glypicans. *Int. J. Biochem. Cell. Biol.*, 35, 125–129.
14. Tumova, S., Woods, A., and Couchman, J.R. (2000). Heparan sulfate proteoglycans on the cell surface: versatile coordinators of cellular functions. *Int. J. Biochem. Cell Biol.*, 32, 269–288.
15. Yoneda, A., and Couchman, J.R. (2003). Regulation of cytoskeletal organization by syndecan transmembrane proteoglycans. *Matrix Biol.*, 22, 25–33.
16. Funakoshi, T., Majima, T., Iwasaki, N., Yamane, S., Masuko, T., Minami, A., Harada, K., Tamura, H., Tokura, S., and Nishimura, S. (2005). Novel chitosan-based hyaluronan hybrid polymer fibers as a scaffold in ligament tissue engineering. *J. Biomed. Mater. Res. A*, 74, 338–346.
17. Adams, J.C. (2002). Regulation of protrusive and contractile cell-matrix contacts. *J. Cell Sci.*, 115, 257–265.
18. Bustin, S.A. (2002). Quantification of mRNA using real-time reverse transcription PCR (RT-PCR): trends and problems. *J. Mol. Endocrinol.*, 29, 23–39.
19. Giulietti, A., Overbergh, L., Valckx, D., Decallonne, B., Bouillon, R., and Mathieu, C. (2001). An overview of real-time quantitative PCR: applications to quantify cytokine gene expression. *Methods*, 25, 386–401.
20. Sherman, L., Sleeman, J., Herrlich, P., and Ponta, H. (1994). Hyaluronate receptors: key players in growth, differentiation, migration and tumor progression. *Curr. Opin. Cell Biol.*, 6, 726–733.
21. Gassler, N., Tugtekin, I., Decker, B., Bosch, U., and Delbruck, A. (1994). Changes in the extracellular matrix of the autogenous patellar tendon graft after posterior cruciate ligament reconstruction: a biochemical study in sheep. *Matrix Biol.*, 14, 87–99.
22. Chen, L., Klass, C., and Woods, A. (2004). Syndecan-2 regulates transforming growth factor-beta signaling. *J. Biol. Chem.*, 279, 15715–15718.
23. Utani, A., Nomizu, M., Matsuura, H., Kato, K., Kobayashi, T., Takeda, U., Aota, S., Nielsen, P.K., and Shinkai, H. (2001). A unique sequence of the laminin alpha 3 G domain binds to heparin and promotes cell adhesion through syndecan-2 and -4. *J. Biol. Chem.*, 276, 28779–28788.
24. Kusano, Y., Oguri, K., Nagayasu, Y., Munesue, S., Ishihara, M., Saiki, I., Yonekura, H., Yamamoto, H., and Okayama, M. (2000). Participation of syndecan 2 in the induction of stress fiber formation in cooperation with integrin alpha5beta1: structural characteristics of heparan sulfate chains with avidity to COOH-terminal heparin-binding domain of fibronectin. *Exp. Cell Res.*, 256, 434–444.
25. Cukierman, E., Pankov, R., Stevens, D.R., and Yamada, K.M. (2001). Taking cell-matrix adhesions to the third dimension. *Science*, 294, 1708–1712.
26. Moulin, V., Castilloux, G., Jean, A., Garrel, D.R., Auger, F.A., and Germain, L. (1996). In vitro models to study wound healing fibroblasts. *Burns*, 22, 359–362.
27. Lee, P.H., Trowbridge, J.M., Taylor, K.R., Morhenn, V.B., and Gallo, R.L. (2004). Dermatan sulfate proteoglycan and glycosaminoglycan synthesis is induced in fibroblasts by transfer to a three-dimensional extracellular environment. *J. Biol. Chem.*, 279, 48640–48646.
28. Knudson, C.B., Nofal, G.A., Pamintuan, L., and Aguiar, D.J. (1999). The chondrocyte pericellular matrix: a model for hyaluronan-mediated cell-matrix interactions. *Biochem. Soc. Trans.*, 27, 142–147.
29. Travis, J.A., Hughes, M.G., Wong, J.M., Wagner, W.D., and Geary, R.L. (2001). Hyaluronan enhances contraction of collagen by smooth muscle cells and adventitial fibroblasts: role of CD44 and implications for constrictive remodeling. *Circ. Res.*, 88, 77–83.
30. Boraldi, F., Croce, M.A., Quaglino, D., Sammarco, R., Carnevali, E., Tiozzo, R., and Pasquali-Ronchetti, I. (2003). Cell-matrix interactions of in vitro human skin fibroblasts upon addition of hyaluronan. *Tiss. Cell.*, 35, 37–45.
31. Huang-Lee, L.L., Wu, J.H., and Nimni, M.E. (1994). Effects of hyaluronan on collagen fibrillar matrix contraction by fibroblasts. *J. Biomed. Mater. Res.*, 28, 123–132.
32. Huang, L., Cheng, Y.Y., Koo, P.L., Lee, K.M., Qin, L., Cheng, J.C., and Kumta, S.M. (2003). The effect of hyaluronan on osteoblast proliferation and differentiation in rat calvarial-derived cell cultures. *J. Biomed. Mater. Res. A*, 66, 880–884.
33. Roy, F., DeBlois, C., and Doillon, C.J. (1993). Extracellular matrix analogs as carriers for growth factors: in vitro fibroblast behavior. *J. Biomed. Mater. Res.*, 27, 389–397.
34. Hu, M., Sabelman, E.E., Lai, S., Timek, E.K., Zhang, F., Hentz, V.R., and Lineaweaver, W.C. (1999). Polypeptide resurfacing method improves fibroblast's adhesion to hyaluronan strands. *J. Biomed. Mater. Res.*, 47, 79–84.
35. Lokeshwar, V.B., Iida, N., and Bourguignon, L.Y. (1996). The cell adhesion molecule, GP116, is a new CD44 variant (ex14/v10) involved in hyaluronic acid binding and endothelial cell proliferation. *J. Biol. Chem.*, 271, 23853–23864.
36. Zimmerman, E., Geiger, B., and Addadi, L. (2002). Initial stages of cell-matrix adhesion can be mediated and modulated by cell-surface hyaluronan. *Biophys. J.*, 82, 1848–1857.
37. Worapamorn, W., Haase, H.R., Li, H., and Bartold, P.M. (2001). Growth factors and cytokines modulate gene expression of cell-surface proteoglycans in human periodontal ligament cells. *J. Cell Physiol.*, 186, 448–456.

# Stabilization of the Proximal Ulnar Stump in the Sauvé-Kapandji Procedure by Using the Extensor Carpi Ulnaris Tendon: Long-Term Follow-Up Studies

**Akio Minami, MD, Norimasa Iwasaki, MD, Jun-ichi Ishikawa, MD, Naoki Suenaga, MD, Hiroyuki Kato, MD**

*From the Department of Orthopaedic Surgery, Hokkaido University School of Medicine, Sapporo, Japan.*

**Purpose:** The Sauvé-Kapandji procedure is considered a useful treatment option for distal radioulnar disorders. Postoperative instability of the proximal ulnar stump and radioulnar convergence, however, may be symptomatic. We modified the Sauvé-Kapandji procedure by stabilizing the proximal ulnar stump with a half-slip of the extensor carpi ulnaris tendon. We previously reported on 13 patients with this procedure at an average follow-up period of 35 months; the patients had satisfactory clinical results and improved stability of the proximal ulnar stump as shown by x-ray examination. In this article we address the question of whether those clinical and radiographic results noted at an average follow-up period of 35 months after surgery were maintained at later follow-up examinations.

**Methods:** We re-examined 12 of the 13 original patients and compared their initial follow-up results with their current results after an average follow-up period of 95 months.

**Results:** The results of this series after 95 months of follow-up evaluation were similar to the results at 35 months.

**Conclusions:** The results presented in this article suggest that the clinical radiographic results at the 35-month follow-up examination were maintained in the long-term 95-month follow-up evaluation despite the finding that the hole in the proximal ulnar stump had broken in 3 wrists at follow-up examination. (J Hand Surg 2006;31A:440–444. Copyright © 2006 by the American Society for Surgery of the Hand.)

**Type of study/level of evidence:** Therapeutic, Level IV.

**Key words:** Extensor carpi ulnaris tendon, stabilization, proximal ulnar stump, Sauvé-Kapandji procedure.

The Sauvé-Kapandji (S-K) procedure is considered a useful treatment option for distal radioulnar disorders.[1–3] Satisfactory clinical results have been obtained in most reports; however, instability of the proximal ulnar stump and radioulnar convergence have caused problems similar to those seen after a Darrach's procedure at average follow-up periods ranging from 29 to 96 months in several articles.[3–6] Instability of the proximal ulna allows convergence of the ulna and radius. Narrowing of the interosseous space allows impingement of the proximal ulnar stump on the distal radial metaphysis. This may cause a painful snapping on rotation, limitation of motion, loss of strength, and occasional bony erosion.

We developed a modification of the S-K procedure to use in the treatment of osteoarthritis (OA) of the distal radioulnar joint (DRUJ). We used a slip of the extensor carpi ulnaris (ECU) tendon to stabilize the proximal ulnar stump.[7] We reported our results with the first 13 patients at a mean average follow-up period of 35 months. The clinical results were satisfactory and x-ray examination suggested that the ECU tendon slip provided a stabilizing effect on the proximal ulnar stump in most patients. We concluded that in the treatment of DRUJ OA stabilization of the proximal ulnar stump with a portion of the ECU tendon should be added to the S-K procedure.[7]

We address here the question of whether clinical and radiographic results noted 35 months after the

procedure are maintained at later follow-up examinations. To answer this question we compared the 35-month follow-up results with our current results obtained an average of 95 months after the procedure in the same patients.

## Patients and Methods

We previously reported the results of 13 wrists with DRUJ OA treated by a modified S-K procedure.[7] Twelve of the 13 wrists from the first group were available for recheck examination. One female patient was lost to follow-up evaluation. The average age of the patients was now 57 years (range, 33–74 y). There were 8 men and 4 women. The length of the follow-up period averaged 95 months (range, 72–131 mo). All the wrists were diagnosed as DRUJ OA (8 primary, 4 traumatic). Rheumatoid arthritis and other diseases of the DRUJ were excluded. X-rays were obtained from the last follow-up examination for each patient.

Before surgery all patients complained of pain in the wrist joint (particularly on forearm rotation), limitation of forearm pronosupination, limitation of wrist extension-flexion, weakness of grip strength, and wrist instability. Tears of the triangular fibrocartilage complex were identified during surgery in all wrists.[8]

We evaluated the clinical results on the following criteria: pain, range of motion (wrist flexion-extension and forearm rotation), grip strength, and return-to-work status. Pain was graded as no pain, slight (cold weather exacerbation), mild (no effect on activity), moderate (affects activity), and severe (frequent pain with light activity).

To evaluate the radiographic findings standard posteroanterior and lateral x-ray films were obtained before and after surgery. Ulnar variance was determined by measuring the distance between lines tangential to the articular surface of the lunate fossa of the radius and the distal articular surface of the ulnar head, which are perpendicular to the longitudinal axis of the forearm.[9]

Radioulnar convergence was determined by comparing the changes in alignment and distance between the radius and ulna from their preoperative to their postoperative status. The interosseous distance between the radius and ulna at the level of the distal end of the proximal ulnar fragment was measured on the posteroanterior films as described by Nakamura et al.[4] Dorsopalmar alignment on the lateral x-ray view was assessed as the perpendicular distance between the dorsal cortices of the radius and ulna at the point of ulnar resection on a true lateral view.[7] The measured point at the preoperative lateral x-ray film, which corresponded to the proximal ulnar stump after the S-K procedure, was estimated retrospectively. An accurate lateral view was defined as the overlapping of the tangents to the palmar cortex of the scaphoid tuberosity and palmar cortex of the capitate. The lateral views were deemed suitable for recording in all cases. If the ulnar stump lay dorsal to the radius a positive value was assigned.

Statistical analysis was calculated using a paired Student *t* test.

### Surgical Procedure

We performed the modified S-K procedure according to a previously described method.[3,7] A small segment of the ulnar shaft and its periosteum was resected proximal to the ulnar head. The corresponding articular surfaces of the DRUJ were decorticated. The resected fragment of the ulna was sculpted to fit into any remaining space between the ulnar head and sigmoid notch. These elements then were fixed by a K-wire and a 3-mm cancellous bone screw.

The stabilization of the proximal ulnar stump then was performed by the method described previously.[7] A 3.5-mm hole was drilled from the dorsoulnar aspect of the ulnar shaft into the intramedullary cavity. The ECU tendon was split in the central sulcus and the radial half was released at the ulnocarpal level. It then was reflected proximally, leaving it attached at the musculotendinous junction. This proximally based strip, approximately 6 to 8 cm long, then was passed into the medullary canal through the drill hole, retrieved at the distal stump of the ulna, pulled distally under moderate tension, and then sutured back on itself in an interlacing fashion.

A long-arm splint was applied for 2 weeks after surgery, after which gentle active motion of the wrist and forearm was encouraged. Full motion of the wrist was allowed after bony fusion of the radioulnar joint was confirmed on x-ray films. The K-wire was left in place in most patients; however, it was removed when skin irritation appeared at the tip of the wire. The K-wire was removed in 2 patients 1 year and 2 years after the S-K procedure.

## Results

### Clinical Results

Pain. All 12 patients complained of pain before surgery (9 severe, 3 moderate). The severity of the pain had improved in all patients at the 35-month follow-up examination and pain had been rated as follows: moderate in 1 patient, slight in 4, and absent in 7. At the final follow-up visit (average, 95 months after the modified S-K procedure) pain was rated as moderate in 1 patient, slight in 3, and absent in 8.

**Table 1. Comparison of Clinical Results at 35- and 95-Month Follow-Up Evaluation (N=12)**

| | Motion (deg) | | |
|---|---|---|---|
| | Preoperative | At 35 mo | At 95 mo |
| Wrist | | | |
| Extension | 47 ± 19* | 56 ± 15 | 53 ± 15 |
| Flexion | 42 ± 15 | 50 ± 13 | 48 ± 13 |
| Forearm | | | |
| Pronation | 68 ± 25 | 81 ± 10 | 78 ± 10 |
| Supination | 63 ± 22 | 77 ± 15 | 78 ± 14 |
| Grip strength (kgf) | 19 ± 13 | 29 ± 15 | 29 ± 15 |

*Average ± standard error.

Motion. The preoperative range of motion of the affected wrist averaged 47° ± 19° (standard error) in extension and 42° ± 15° in flexion. At the 35-month follow-up examination the extension averaged 56° ± 15° and flexion averaged 50° ± 13°. These improvements were not statistically significant. After an average of 95 months the extension averaged 53° ± 15° and flexion averaged 48° ± 13° (Table 1).

The preoperative forearm motion averaged 68° ± 25° in pronation and 63° ± 22° in supination. At the 35-month follow-up examination pronation averaged 81° ± 10° and supination averaged 77° ± 15°. Both postoperative improvements were statistically significant ($p < .05$). After an average of 95 months of follow-up evaluation pronation averaged 78° ± 10° and supination averaged 78° ± 14°.

There were no statistically significant differences with regard to range of motion (wrist extension-flexion, forearm pronation-supination) between the 35-month and the 95-month follow-up examinations.

Grip strength. The preoperative grip strength of the affected wrist averaged 19 ± 13 kgf (61% of the contralateral side) (Table 1). After surgery the grip strength of the affected wrist at the 35-month follow-up visit averaged 29 ± 15 kgf (90%). All wrists had an increased grip strength over the preoperative value with a statistical value of p less than .005. At an average of 95 months after the procedure grip strength averaged 29 ± 15 kgf. This comparison suggests that the postoperative results at 35 months were maintained at 95 months.

Work status. Eleven patients returned to their previous occupations. One patient returned to light work but had no difficulty with functions of daily living and his avocation at the time of the 35-month follow-up examination. At an average of 95 months after the procedure 1 patient retired from his occupation. Ten patients, however, continued the same occupation including that of housekeeping.

X-ray evaluations. Eleven of the 12 wrists had positive ulnar variance with an average of 3 mm (range, 2–8 mm) before surgery. Postoperative ulnar variance averaged 0.2 mm (range, −1 to 1 mm).

Fusion of the DRUJ was confirmed by x-ray examination in all wrists within 10 weeks after surgery. The preoperative radioulnar distance averaged 14 ± 31 mm. The postoperative distance at the 35-month follow-up examination measured 13 ± 3 mm. There was no statistical significance between them. At an average of 95 months after the procedure the radioulnar distance was 12 ± 4 mm. The proximal ulnar stump did not impinge on the radius directly in any instance. At the final follow-up evaluation the proximal ulnar stump had tapered proximally and hypertrophied distally in all cases. These results suggested that postoperative radioulnar convergence was diminished or prevented even after a long-term follow-up evaluation.

The preoperative measures of the dorsopalmar distance were 6 ± 4 mm whereas the postoperative measures at the 35-month follow-up examination averaged 1 ± 2 mm ($p < .01$). At the 95-month follow-up evaluation the postoperative measurements were 2 ± 2 mm. There was no statistically significant difference between the values at the 35- and 95-month follow-up examinations although there was slight tendency of dorsalward migration of the proximal ulnar stump at the final follow-up examination. These results suggest that the stabilization procedure had a positive effect on reduction of the dorsal subluxation of the proximal ulnar stump after the S-K procedure.

Breakage of the drilled hole was found in 3 wrists at the 95-month follow-up examination; however, the instability of the proximal ulnar stump was not marked in these 3 wrists.

These overall results suggest that the clinical and radiographic results at the 35-month follow-up examination were maintained at the final follow-up visit.

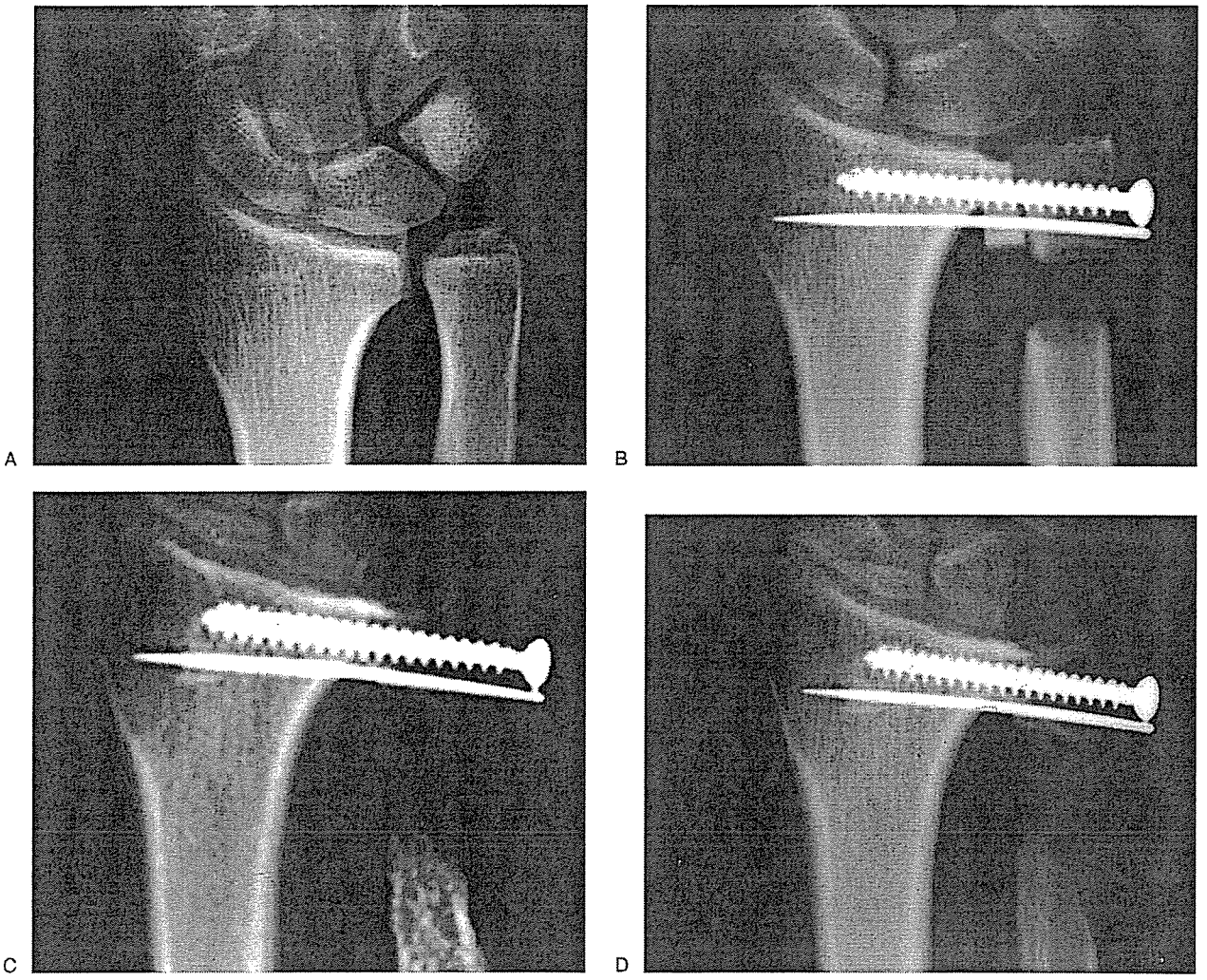


**Figure 1.** (A) Preoperative x-ray film showed slight DRUJ OA and a neutral ulnar variance. The ulnar head had been trimmed by a wafer procedure. (B) Posteroanterior x-ray film 2 weeks after the modified S-K procedure with stabilization of the proximal ulnar stump with a half-slip of the ECU tendon. (C) Posteroanterior x-ray film 3 years and 5 months after the procedure showing good alignment of the proximal ulnar stump without any convergence toward the radius. (D) Posteroanterior x-ray film 8 years and 6 months after the procedure showing that the pseudoarthrosis gap of the ulna was well preserved and that the stability of the proximal ulnar stump also was preserved, although the proximal ulnar stump was tapered.

## Case Report

A 37-year-old man had increasing pain in the right wrist associated with work without any trauma. The patient was diagnosed with an ulnar impingement syndrome. Although 6-month conservative treatments including splinting and injections of corticosteroids were applied, the pain did not improve. The wafer procedure was performed by the open method. Surgical findings showed chondromalacia on the ulnar head and the proximal articular surface of the lunate and moderate degenerative changes on the DRUJ; however, there was no clinical improvement. Preoperative x-ray film showed slight osteoarthritis of the DRUJ and neutral ulnar variance (Fig. 1A). Pain was severe. The patient had 30° extension and 40° flexion at the wrist, with 70° pronation and 30° supination of the forearm.

Grip strength of the right wrist was 15 kgf (left, 45 kgf). The modified S-K procedure with stabilization of the proximal ulnar stump with a slip of the ECU tendon was performed (Fig. 1B). The postoperative course was uneventful. Bone union between the radius and ulna occurred 8 weeks after the procedure. The patient had complete pain relief 6 months after the procedure. X-ray film 3 years and 5 months after the procedure showed good alignment of the proximal ulnar stump without any convergence toward the radius (Fig. 1C). Eight years and 6 months after the procedure the range of motion was 70° extension and 60° flexion of the wrist and 80° pronation and 90° supination of the forearm. Grip strength increased to 40 kgf. X-ray examination showed that the pseudoarthrosis gap of the ulna was well preserved and the

alignment of the proximal ulnar stump was acceptable (Fig. 1D).

## Discussion

The S-K procedure has a reputation of being a reliable and effective method of dealing with distal radioulnar disorders.[1–7,10,11] De Smet and Van Ransbeeck[12] reported the outcome of the S-K procedure for posttraumatic wrist disorders. Eighty-four patients were treated, all with posttraumatic disorders of the DRUJ. There was a marked decrease in pain and a high rate of patient satisfaction (74%). The postoperative range of motion improved significantly in the flexion-extension arc and the pronation-supination arc. We also reported our clinical results of the S-K procedure performed in 13 patients with primary and secondary OA of the DRUJ.[3] Postoperative pain relief was good in all wrists. After surgery the flexion-extension arc improved, although no statistical significance was shown when compared with the preoperative values. There was a postoperative statistical improvement of the pronation-supination arc.

On x-ray examination we saw some evidence of unstable proximal ulnar stumps and radioulnar convergence in all patients similar to that associated with the Darrach's procedure.[3,4] We reported that the postoperative x-ray evaluation showed an unstable proximal ulnar stump and radioulnar convergence in 12 of 13 wrists.[3] Dorsal and radial instability of the proximal ulnar stump may be a major complication of the S-K procedure.

Several procedures have been proposed to improve the stability of the proximal ulnar stump after the S-K procedure.[7,13–16] We developed a stabilization procedure for the S-K procedure as a result of our early experience in the treatment of OA of the DRUJ. We used a slip of the ECU tendon as a dynamic tether to the proximal ulnar stump.[7] Postoperative x-rays in our late series showed improved alignment in both coronal and lateral planes.

Our method is very simple and does not require extension of the surgical field. We have extended our surgical indications from OA of the DRUJ to other radioulnar disorders on the basis of our results to date, but these results will be followed up further to see if the beneficial results persist.

The authors thank Ronald L. Linscheid, MD, Professor Emeritus, Surgery of the Hand, Department of Orthopaedics, Mayo Clinic, Rochester, MN, for his suggestions during this investigation.

Received for publication May 17, 2005; accepted in revised form November 1, 2005.

No benefits in any form have been received or will be received from a commercial party related directly or indirectly to the subject of this article.

Corresponding author: Akio Minami, MD, Department of Orthopaedic Surgery, Hokkaido University School of Medicine, Kita-15-jo, Nishi-7-chome, Kita-ku, Sapporo, 060-8638, Japan; e-mail: a-minami@med.hokudai.ac.jp.



0363-5023/06/31A03-0013$32.00/0
doi:10.1016/j.jhsa.2005.11.012

## References

1. Goncalves D. Correction of disorders of the distal radio-ulnar joint by artificial pseudarthrosis of the ulna. J Bone Joint Surg 1974;56B:462–464.
2. Kapandji IA. The Kapandji-Sauve operation. Its techniques and indications in nonrheumatoid diseases. Ann Chir Main 1986;5:181–193.
3. Minami A, Suzuki K, Suenaga N, Ishikawa J. The Sauve-Kapandji procedure for osteoarthritis of the distal radioulnar joint. J Hand Surg 1995;20A:602–608.
4. Nakamura R, Tsunoda K, Watanabe K, Horii E, Miura T. The Sauve-Kapandji procedure for chromic dislocation of the distal radio-ulnar joint with destruction of the articular surface. J Hand Surg 1992;17B:127–132.
5. Zimmermann R, Gschwentner M, Arora R, Harpf C, Gabl M, Pechlaner S. Treatment of distal radioulnar joint disorders with a modified Sauve-Kapandji procedure: long-term outcome with special attention to the DASH questionnaire. Arch Orthop Trauma Surg 2003;123:293–298.
6. George MS, Kiefhaber TR, Stern PJ. The Sauve-Kapandji procedure and the Darrach procedure for distal radio-ulnar joint dysfunction after Colles' fracture. J Hand Surg 2004; 29B:608–613.
7. Minami A, Kato H, Iwasaki N. Modification of the Sauve-Kapandji procedure with extensor carpi ulnaris tenodesis. J Hand Surg 2000;25A:1080–1084.
8. Palmer AK. Triangular fibrocartilage complex lesions: a classification. J Hand Surg 1989;14A:594–606.
9. Palmer AK, Glisson RR, Werner FW. Ulnar variance determination. J Hand Surg 1982;7:376–379.
10. Millroy P, Coleman S, Ivers R. Sauve-Kapandji operation. Technique and results. J Hand Surg 1992;17B:411–414.
11. Carter PB, Stuart PR. The Sauve-Kapandji procedure for post-traumatic disorders of the distal radio-ulnar joint. J Bone Surg 2000;82B:1013–1018.
12. De Smet LA, Van Ransbeeck H. The Sauve-Kapandji procedure for posttraumatic wrist disorders: further experience. Acta Orthop Belg 2000;66:251–254.
13. Rothwell AG, O'Neill L, Cragg K. Sauve-Kapandji procedure for disorders of the distal radioulnar joint: a simplified technique. J Hand Surg 1996;21A:771–777.
14. Lamey DM, Fernandez DL. Results of the modified Sauve-Kapandji procedure in the treatment of chronic posttraumatic derangement of the distal radioulnar joint. J Bone Joint Surg 1998;80A:1758–1769.
15. Couturier C, Alnot JY, Masmejean E. Dorsal instability of the ulnar stump following distal resection: hemi extensor-carpi-ulnaris stabilization procedure. Chir Main 2002;21: 242–251.
16. Low CK, Chew WY. Results of Sauve-Kapandji procedure. Singapore Med J 2002;43:135–137.